Desalination and Water Treatment
www.deswater.com

doi: 10.5004/dwt.2018.22891

126 (2018) 224–230
September

Effects of calcination temperature on photocatalytic degradation of ofloxacin on $Gd_2Ti_2O_7$/HZSM-5

Wenjie Zhang*, Yinghao Dong, Chuanguo Li

School of Environmental and Chemical Engineering, Shenyang Ligong University, Shenyang 110159, China, Tel. +86 13609880790, emails: wjzhang@aliyun.com (W. Zhang), 470735504@qq.com (Y. Dong), 812668907@qq.com (C. Li)

Received 6 January 2018; Accepted 29 July 2018

ABSTRACT

$Gd_2Ti_2O_7$ was supported on HZSM-5 zeolite by sol-gel method to investigate the effects of calcination temperature on the properties of the $Gd_2Ti_2O_7$/HZSM-5 composite. The crystallization of pyrochlore $Gd_2Ti_2O_7$ phase starts at 750°C, with the most preferred orientation at the (222) plane. The absorptions of the metal-oxide bondings in gadolinium titanate can be seen in the far infrared spectra of the crystallized $Gd_2Ti_2O_7$. The shrinking band gap energy at high calcination temperature can be attributed to the growth of $Gd_2Ti_2O_7$ grain. IUPAC type IV adsorption–desorption isotherm and type H3 hysteretic loop in the isotherms indicate mesoporous structure with broad pore size distribution in the $Gd_2Ti_2O_7$/HZSM-5 composites. Adsorption of ofloxacin on the composite decreases with rising calcination temperature, which is in accordance to the change in surface area. The $Gd_2Ti_2O_7$/HZSM-5 sample calcined at 800°C has the maximum activity on ofloxacin degradation. Well-crystallized $Gd_2Ti_2O_7$ has good activity, while the shrinking surface area and porosity at high temperature are detrimental to its activity.

Keywords: $Gd_2Ti_2O_7$; Photocatalytic; HZSM-5; Ofloxacin; Degradation

1. Introduction

Wastewater containing antibiotics has to be treated before discharging into aquatic system. Advanced oxidation methods such as photocatalytic technique are capable of removing antibiotics from wastewater, and many kinds of antibiotics can be deeply oxidized in this way to reduce the potential hazard to ecosystem [1–4]. Titania-based material is the largest type of photocatalytic material throughout decades of investigation [5–7]. On the other hand, the researchers have paid much efforts in developing novel and powerful materials. Titanates in pyrochloro and perovskite structures have grown to be a big group of potential photocatalytic material [8–12]. Khodadoost et al. [13] reported hydrothermal synthesis of bismuth titanate nanoparticles and application for photocatalytic degradation of tetracycline.

Titanate is distinguished by the cation elements in the formula, such as alkaline earth metals and lanthanide elements. Different preparation methods are studied to prepare $La_2Ti_2O_7$, such as hydrothermal method and solid state reaction [14,15]. Zhang et al. [16] reported sol-gel synthesis of $Dy_2Ti_2O_7$ nanocrystalline. Photocatalyst is usually not applied in the powder form during water treatment. Supported form is often needed to facilitate actual wastewater treating process, for example, solid–liquid separation after treatment. HZSM-5 zeolite is a kind of porous structured material that has large surface area. It is utilized as adsorbent, catalyst and support for many purposes. Guo et al. [17] and Kumari et al. [18] also reported the promoted photocatalytic activity of TiO_2 after supporting on HZSM-5. We used HZSM-5 zeolite to support TiO_2 [19], $SrTiO_3$ [20] and $La_2Ti_2O_7$ [8] in our previous work. Photocatalytic activities of the above-mentioned materials are greatly enhanced after loading on HZSM-5 zeolite.

* Corresponding author.

In this work, $Gd_2Ti_2O_7$ was supported on HZSM-5 zeolite by sol-gel method to prepare composite $Gd_2Ti_2O_7$/HZSM-5. The materials were characterized using X-ray powder diffraction, scanning electron microscopy, Fourier transform infrared/far infrared spectroscopy, UV–Visible spectrometry, and surface area and pore size analyzes. The effects of calcination temperature on ofloxacin removal efficiencies through adsorption and photocatalytic degradation on $Gd_2Ti_2O_7$/HZSM-5 were studied.

2. Experimental setup

2.1. Synthesis of $Gd_2Ti_2O_7$/HZSM-5

A typical sol-gel route was used to support $Gd_2Ti_2O_7$ on HZSM-5 particles. 0.85 mL tetrabutyl titanate was dissolved in 8 mL ethanol to prepare solution A. 1.1284 g $Gd(NO_3)_3 \bullet 6H_2O$ and 8 mL acetic acid were dissolved in 8 mL deionized water to prepare solution B. Solution B was slowly added into solution A under stirring to produce a transparent sol, followed by addition of HZSM-5 particles. The *n*(Gd):*n*(Ti) ratio was 1:1 in the sol. Transformation from sol to gel happened after 2 h in a 70°C water bath. The gel was dehydrated at 110°C for 15 h. Thermal treatment to the powders was conducted in a furnace for 3 h. Calcination temperature was indicated in the subsequent section. The product was ground and named as $Gd_2Ti_2O_7$/HZSM-5, which contained 90% of $Gd_2Ti_2O_7$ in the composite.

2.2. Characterization methods

Crystal structures of the materials were analyzed by D8 Advance X-ray diffractometer with Cu Kα radiation. Surface morphologies of the materials were measured on QUANTA 250 scanning electron microscope. Infrared and far infrared absorption spectra were determined by Frontier FT-IR/FIR spectrometer. UV–Vis diffuse reflectance spectra were recorded by LAMBDA 35 UV–Vis spectrometer. An integrating sphere was equipped to determine the reflectance intensity. Kubelka and Munk [21] method was used to transform reflection intensity to absorbance. Specific surface area and porous structure measurements were performed on ASAP 2460 surface area and pore size analyzer. The specific surface area was determined by the multipoint BET method. Pore size distribution was determined using the Barrett, Joyner, and Halenda method.

2.3. Adsorption and photocatalytic degradation measurements

Adsorption and photocatalytic degradation of ofloxacin were examined in this work to evaluate the removal efficiency on $Gd_2Ti_2O_7$/HZSM-5. 50 mL ofloxacin solution and 20 mg $Gd_2Ti_2O_7$ were mixed in a quartz beaker and stirred in the dark to ensure adsorption–desorption equilibrium. The initial ofloxacin solution concentration was 20 mg/L. A 20 W UV lamp was used as the UV irradiation source with the irradiation intensity of 2,300 μW/cm^2 at 253.7 nm, which was measured at the surface of the ofloxacin solution. After high-speed centrifuge and filtration, the filtrate was examined on Agilent 1260 high performance liquid chromatography equipped with Zorbax Eclipse XDB-C18 (150 × 4.6 mm) column. *V*(1% phosphoric acid aqueous solution): *V*(acetonitrile) in the mobile phase was 80%:20%. The absorption intensity of ofloxacin was measured at 294 nm on the UV detector.

3. Results and discussion

3.1. Characterization of $Gd_2Ti_2O_7$/HZSM-5

$Gd_2Ti_2O_7$/HZSM-5 composite contains 90% $Gd_2Ti_2O_7$ and 10% HZSM-5. HZSM-5 has no photocatalytic activity and acts to support $Gd_2Ti_2O_7$ in the composite. The major constitute in $Gd_2Ti_2O_7$/HZSM-5 is $Gd_2Ti_2O_7$, whose properties are affected by the minor HZSM-5 particles. High temperature thermal treatment is necessary to form crystallite $Gd_2Ti_2O_7$. Fig. 1 shows X-ray diffraction patterns of $Gd_2Ti_2O_7$/HZSM-5 as a factor of calcination temperature. HZSM-5 is very stable during thermal treatment, and its diffraction pattern does not change with calcination temperature. The diffraction peaks of HZSM-5 are hardly found in the XRD patterns of $Gd_2Ti_2O_7$/HZSM-5 composites since HZSM-5 particles are coated with a thick layer of $Gd_2Ti_2O_7$.

As can be seen from the figure, gadolinium titanate is in the amorphous state at low calcination temperature, and crystallization of $Gd_2Ti_2O_7$ begins at 750°C. At higher temperatures, the only substance formed in the materials is $Gd_2Ti_2O_7$ in pyrochlore structure, whose diffraction patterns are in accordance to that of PDF No. 73-1698. The most preferred orientation is the (222) plane of the pyrochlore $Gd_2Ti_2O_7$ phase that is stable during thermal treatment at temperature as high as 1,000°C. There is no transformation of pyrochlore $Gd_2Ti_2O_7$ to other kinds of substances at the temperatures indicated in Fig. 1. Lattice parameters, cell volume and grain size of $Gd_2Ti_2O_7$/HZSM-5 are calculated based on the diffraction patterns, as shown in Table 1. Cell expansion can be observed with rising calcination temperature. Grain sizes at the (222) plane are 31.6, 56.0 and 73.2 nm at 800°C, 900°C and 1,000°C, respectively.

Fig. 2 shows SEM images of $Gd_2Ti_2O_7$/HZSM-5 at different calcination temperatures. As can be seen from the figures, $Gd_2Ti_2O_7$/HZSM-5 tends to aggregate into large particles

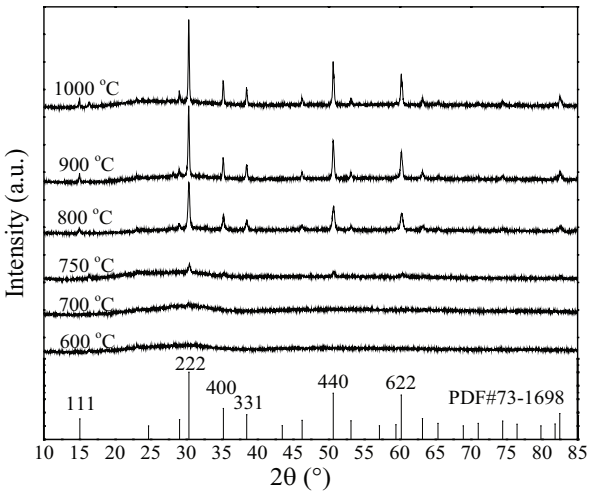

Fig. 1. XRD patterns of $Gd_2Ti_2O_7$/HZSM-5 calcined at different temperatures.

Table 1
Lattice parameters, cell volume and grain size of $Gd_2Ti_2O_7$/HZSM-5

Calcination temperature (°C)	$a = b = c$ (nm)	V (nm^3)	Grain size (nm)
800	1.0184	1.0561	31.6
900	1.0189	1.0577	56.0
1,000	1.0190	1.0581	73.2

in the size of several micrometers. As shown in Fig. 2(g), HZSM-5 particles have regular shape in the size below 5 μm, and the surface morphology of HZSM-5 particles is smooth. Since $Gd_2Ti_2O_7$/HZSM-5 composite contains 90% $Gd_2Ti_2O_7$, HZSM-5 particles are surrounded by a thick $Gd_2Ti_2O_7$ layer, so that the shape of HZSM-5 particles can hardly be distinguished in the figures. Surface morphology of the aggregated $Gd_2Ti_2O_7$/HZSM-5 particles is rough since the $Gd_2Ti_2O_7$ layer is composed of small particles. The HZSM-5 particles seem to act as condensation nuclei during sol-gel process, while

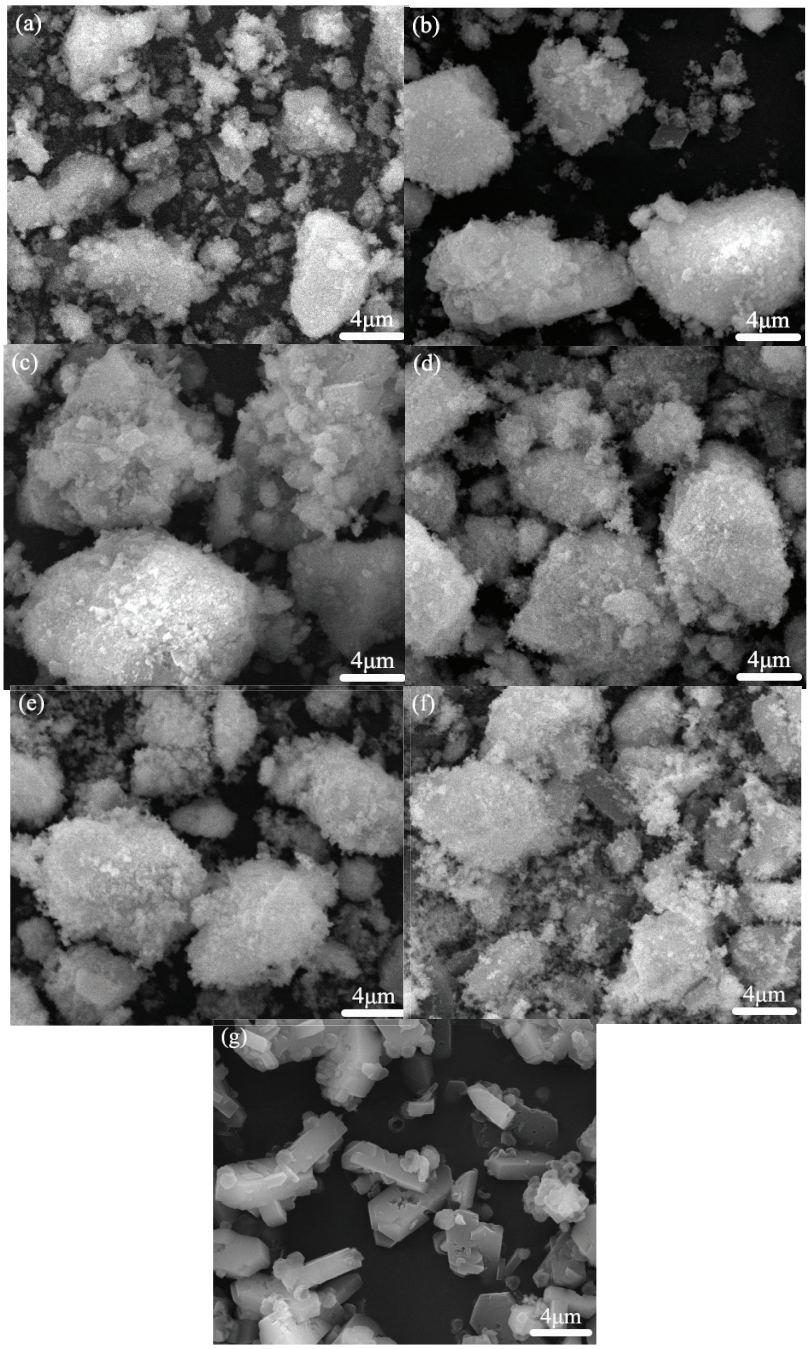

Fig. 2. SEM images of $Gd_2Ti_2O_7$/HZSM-5 at different calcination temperatures. (a) 600°C, (b) 700°C, (c) 750°C, (d) 800°C, (e) 900°C, (f) 1,000°C, (g) HZSM-5.

dehydration of small sol molecules leads to the extension of gel network.

Fig. 3 shows FT-IR and FT-Far IR spectra of $Gd_2Ti_2O_7$/HZSM-5. The typical stretching vibration of hydroxyl group has absorption at 3,433 cm^{-1} [22], and the absorption peak at 1,640 cm^{-1} is attributed to the surface adsorbed water molecules. These two absorption peaks slightly shrink with rising calcination temperature. Anti-symmetric stretching vibration of Al–O–Al or Si–O–Si situates at 1,232 cm^{-1}, while bending vibration of Si–O–Si bond has an absorption at 796 cm^{-1}. The strong absorption at 1,060 cm^{-1} is attributed to stretching vibration of Si(Al)–O in HZSM-5, while anti-symmetric stretching vibration peak of the typical double penta-ring in HZSM-5 situates at 554 cm^{-1} [23]. The above-mentioned absorptions indicate the existence of HZSM-5 in the composite samples.

The absorptions of metal-oxide bondings in gadolinium titanate can be better found in the far infrared spectra, as shown in Fig. 3(b). Absorption peaks of stretching vibrations of Si–O bond and Ti–O bond in octahedral TiO_6 overlaps around 467 cm^{-1} [24]. Absorptions of Gd–O bond do not appear at low calcination temperature, whereas such absorption peaks can be found in the spectra after crystallization of $Gd_2Ti_2O_7$. Absorption at 416 cm^{-1} is due to stretching vibration of Gd–O bond [25,26], and bending vibration of O–Gd–O bond appears at 306 cm^{-1} [25]. The characteristic stretching vibration of Gd-TiO_6 centering at 207 cm^{-1} begins to appear in the sample calcined at 750°C.

UV–Vis diffuse reflectance spectra of $Gd_2Ti_2O_7$/HZSM-5 composites are shown in Fig. 4. Band edges of all the samples are in the ultraviolet region, and band energy of the materials can be affected by the variation of calcination temperature. There is a red shift of the band edge with increasing calcination temperature. Band gap energy of $Gd_2Ti_2O_7$/HZSM-5 composite is calculated from the UV–Vis diffuse reflectance spectra. The $(\alpha h\nu)^2$-$h\nu$ plot inserted in Fig. 4 is drawn based on the formula $(\alpha h\nu) = A(h\nu - Eg)^n$, where α, h, ν, A and Eg are the absorption coefficient, Planck's constant, light frequency, proportionality constant and bandgap energy, respectively [27]. Band gap energies of $Gd_2Ti_2O_7$/HZSM-5 calcined at 600°C, 700°C, 800°C, 900°C and 1,000°C are 3.63, 3.63, 3.60, 3.43 and 3.31 eV, respectively. The shrinking band gap energy can be attributed to grain growth at high temperature, which can be explained by quantum size effect.

N_2 adsorption–desorption isotherms on $Gd_2Ti_2O_7$/HZSM-5 composites are presented in Fig. 5(a). The amount of N_2 adsorbed on $Gd_2Ti_2O_7$/HZSM-5 samples decreases with rising calcination temperature. All the isotherms can be identified as IUPAC type IV, indicating mesoporous structure in the materials. The adsorbed N_2 amount slightly increases with rising N_2 relative pressure before the turning point, after which an abrupt enhancement in the adsorbed N_2 amount occurs at high relative pressure. Monolayer or multilayer N_2 molecules are adsorbed on the surface of $Gd_2Ti_2O_7$/HZSM-5 composite at low pressure, while capillary condensation of N_2 molecules is responsible for the abrupt enlarging adsorption amount. The hysteretic loop in the adsorption–desorption isotherm is a typical character of mesoporous material. Pore

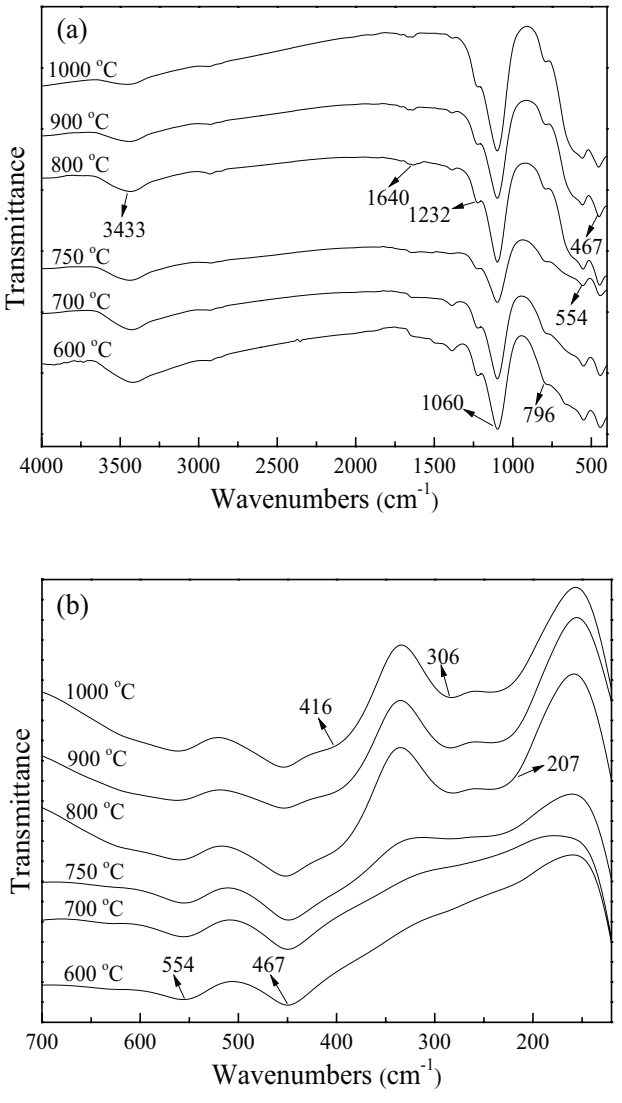

Fig. 3. (a) FT-IR and (b) FT-FIR spectra of $Gd_2Ti_2O_7$/HZSM-5 at different calcination temperatures.

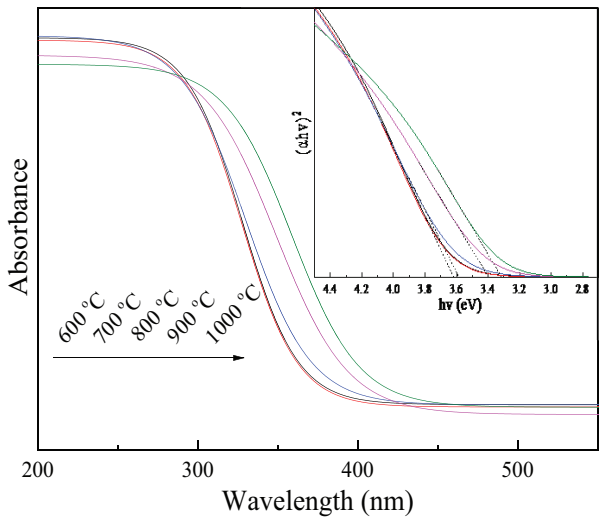

Fig. 4. UV–Vis diffuse reflectance spectra of $Gd_2Ti_2O_7$/HZSM-5 with the variation of calcination temperature.

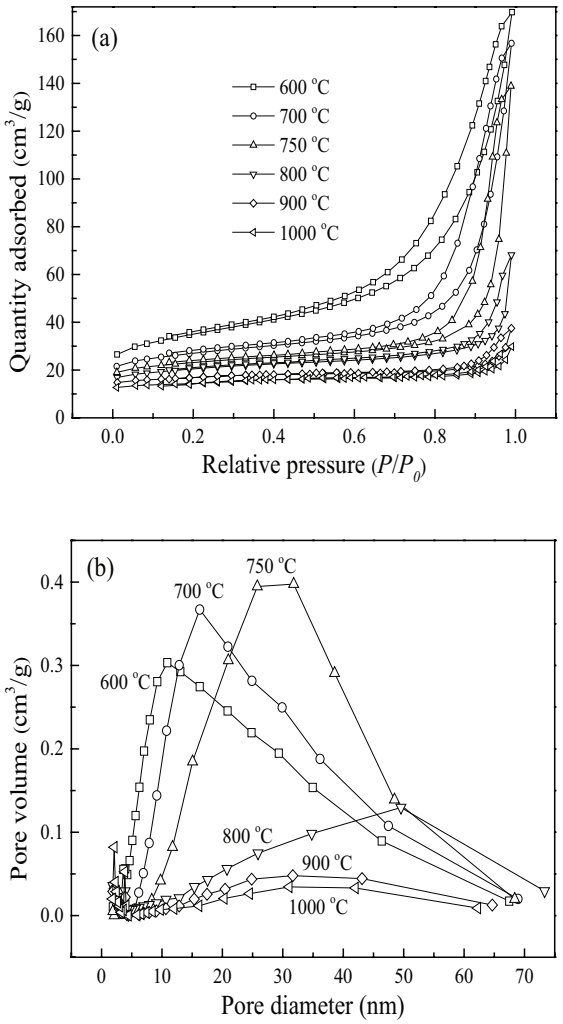

Fig. 5. (a) N_2 adsorption–desorption isotherms and (b) pore size distributions of $Gd_2Ti_2O_7$/HZSM-5 with respect to calcination temperature.

size distribution in the $Gd_2Ti_2O_7$/HZSM-5 composite may be in a wide range, which can be proven by the type H3 hysteretic loop in the isotherms.

Pore size distribution of $Gd_2Ti_2O_7$/HZSM-5 with respect to calcination temperature is illustrated in Fig. 5(b). Despite the difference in calcination temperature, pore size of all the samples is in mesoporous range. The amorphous samples contain large pore volume, and high temperature calcination leads to a sharp loss of pore volume in the material. Crystal growth and particles aggregation at high temperature are responsible for decreasing pore volume.

Table 2 gives specific surface area, average pore size and pore volume of $Gd_2Ti_2O_7$/HZSM-5 composites. These characters have close relationship to calcination temperature. BET surface area reduces from 116.6 to 45.5 m^2/g when calcination temperature increases from 600°C to 1,000°C. Total pore volume is also reduced at high calcination temperature. The $Gd_2Ti_2O_7$/HZSM-5 composite contains 10% HZSM-5 and 90% $Gd_2Ti_2O_7$. The HZSM-5 zeolite is stable at the mentioned thermal treating temperature. Meanwhile, HZSM-5 particles are surrounded by a thick layer of $Gd_2Ti_2O_7$. The variations

Table 2
Specific surface area, average pore size and pore volume of $Gd_2Ti_2O_7$/HZSM-5 as a factor of calcination temperature

Calcination temperature (°C)	BET surface area (m^2/g)	Average pore size (nm)	Pore volume (cm^3/g)
600	116.6	11.9	0.1984
700	87.5	17.5	0.1618
800	66.0	13.6	0.0554
900	53.4	9.8	0.0380
1,000	45.5	6.4	0.0323

of BET surface area and pore volume are mostly due to the effects of calcination temperature on the supported gadolinium titanate.

The amorphous phase has large specific surface area and pore volume. Crystal growth and particles aggregation at high temperature lead to reduction in interparticle holes. Average pore size in the $Gd_2Ti_2O_7$/HZSM-5 composites is in the mesoporous range. The decline of average pore size at calcination temperature over 700°C is attributed to diminish of the porous structure in $Gd_2Ti_2O_7$ layer, since at the same time, the micropores in HZSM-5 zeolite are not changed with the variation of calcination temperature.

3.2. Photocatalytic activity

Photocatalytic oxidation process is initiated from photogeneration of electrons and holes, followed by production of oxidative reagents such as hydroxyl radical. Hydroxyl radical is a powerful oxidizing reagent for oxidation of organic substances. The quantum efficiency on hydroxyl production is in close relationship to the activity of photocatalyst. Terephthalic acid can be oxidized by hydroxyl radical to form 2-hydroxy-terephthalic acid. Fluorescence intensity of 2-hydroxy-terephthalic acid solution after excitation can be used to measure the concentration of hydroxyl radical produced during photocatalytic process. Fig. 6 illustrates fluorescence spectra of terephthalic acid solution after 30 min of irradiation in presence of $Gd_2Ti_2O_7$/HZSM-5 to show the effect of calcination temperature. The amorphous samples calcined at 600°C and 700°C have the lowest quantum efficiency on hydroxyl production. On the other hand, the samples calcined at 800°C and 900°C have nearly the same efficiency.

Fig. 7 illustrates the effects of calcination temperature on adsorption and photocatalytic degradation of ofloxacin on $Gd_2Ti_2O_7$/HZSM-5. Total removal of ofloxacin is composed of adsorption and photocatalytic degradation. 14.7% of ofloxacin molecules are adsorbed on the surface of the pure $Gd_2Ti_2O_7$ in the solution after adsorption–desorption equilibrium, and the adsorbed amount is 15.3% on the $Gd_2Ti_2O_7$/HZSM-5 composite. The adsorption capacity is only 4.1% when solely HZSM-5 zeolite is used. Obviously, the loaded $Gd_2Ti_2O_7$ in the $Gd_2Ti_2O_7$/HZSM-5 composite plays the major role in adsorbing ofloxacin. Adsorption of ofloxacin on the composite decreases with rising calcination temperature, which is in accordance to the variation of BET surface area. The HZSM-5 particles can hardly adsorb ofloxacin, and most of ofloxacin

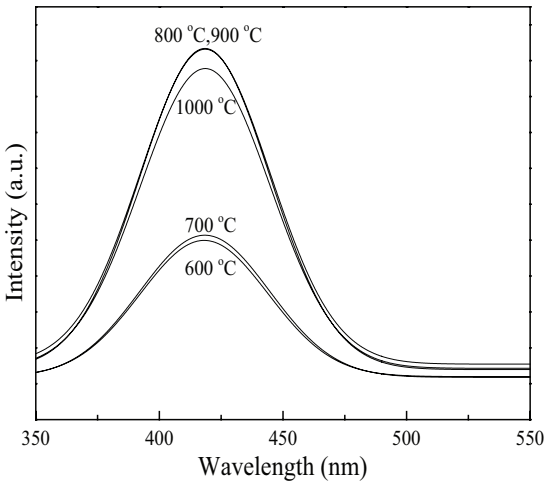

Fig. 6. Fluorescence spectra of terephthalic acid solution after 30 min of irradiation in presence of $Gd_2Ti_2O_7$/HZSM-5 calcined at different temperatures.

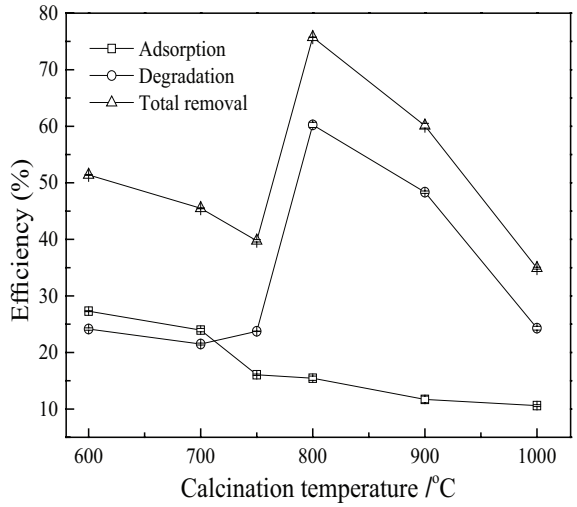

Fig. 7. Effects of calcination temperature on adsorption and photocatalytic degradation of ofloxacin on $Gd_2Ti_2O_7$/HZSM-5.

molecules are adsorbed on the surface of $Gd_2Ti_2O_7$ layer. The amorphous $Gd_2Ti_2O_7$/HZSM-5 prepared at low temperature has large porous structure and surface area.

Photolysis of ofloxacin is quite small and can be ignored in this work, and the HZSM-5 zeolite has no photocatalytic activity either. 27.5% ofloxacin molecules are degraded on the pure $Gd_2Ti_2O_7$ after 30 min of UV irradiation, while the photocatalytic degradation efficiency on the $Gd_2Ti_2O_7$/HZSM-5 composite calcined at 800°C is 60.3% after the same time. The photocatalytic activity of $Gd_2Ti_2O_7$ is enhanced after loading, which is mostly attributed to the well dispersion of $Gd_2Ti_2O_7$ on the surface of HZSM-5 zeolite.

However, the amorphous sample also has poor photocatalytic activity on ofloxacin degradation. As illustrated in XRD patterns, crystallization of pyrochlore $Gd_2Ti_2O_7$ phase starts at 750°C. The $Gd_2Ti_2O_7$/HZSM-5 sample calcined at 800°C has the maximum activity on ofloxacin degradation, while there is abrupt decline of photocatalytic degradation efficiency on the samples calcined at higher temperature. As indicated before, crystal growth and particles aggregation at high temperature lead to shrinking surface area and porous structure in $Gd_2Ti_2O_7$/HZSM-5. Both adsorption capacity and photocatalytic activity of $Gd_2Ti_2O_7$/HZSM-5 depend on porous properties of the supported $Gd_2Ti_2O_7$ layer.

Although adsorption of ofloxacin on the material can partly contribute to the total removal efficiency, ofloxacin can only be degraded through photocatalytic oxidation process. Photocatalytic degradation of ofloxacin is initiated by the adsorption of irradiating photons by the photocatalyst to generate electrons and holes. The charge carriers may migrate to the external surface of the photocatalyst, where they are involved in the oxidation of ofloxacin molecules. The photogenerated electrons then react with molecular oxygen (O_2) to produce superoxide radical anions ($\bullet O_2^-$), and the photogenerated holes react with water to produce hydroxyl radicals (•OH). These two types of reactive radicals work together to decompose ofloxacin molecules that are adsorbed on the surface of the photocatalyst. Complete decomposition of ofloxacin can be achieved after enough irradiation time. Reduced aggregation of $Gd_2Ti_2O_7$ particles and enlarged surface area of $Gd_2Ti_2O_7$ layer in the $Gd_2Ti_2O_7$/HZSM-5 are favored by light absorption to initiate photocatalytic generation of charge carriers.

Photocatalytic degradation of ofloxacin on the $Gd_2Ti_2O_7$/HZSM-5 composite with extending irradiation time was investigated to achieve complete decomposition of ofloxacin in the solution. All of the ofloxacin molecules were degraded after 90 min of photocatalytic reaction. The degradation process obeys the first order reaction law, and the reaction rate constant is 3.52×10^{-2} min^{-1}. The activity of the $Gd_2Ti_2O_7$/HZSM-5 composite is stable during the whole process.

The $Gd_2Ti_2O_7$/HZSM composite calcined at 800°C was reused to examine its recycling performance on ofloxacin degradation. The ofloxacin solution was restored to the initial concentration after 30 min of irradiation in each cycle. Photocatalytic degradation efficiencies are 60.3% and 53.6% in the first cycle and in the fifth cycle. The slight decrease in ofloxacin degradation efficiency is mainly attributed to the loss of fine $Gd_2Ti_2O_7$ powders when taking solution sample for examination.

3.3. Relations between catalyst structure/properties and photocatalytic activity

The purpose of this work is to show the effects of calcination temperature on ofloxacin removal efficiencies through adsorption and photocatalytic degradation on $Gd_2Ti_2O_7$/HZSM-5. The HZSM-5 zeolite seems to be an appropriate material to support $Gd_2Ti_2O_7$ since it has no photocatalytic activity. This microporous zeolite can only adsorb a little amount of ofloxacin too. In this case, the enhanced photocatalytic activity of the loaded $Gd_2Ti_2O_7$ can only be attributed to the changes in the structure and properties of $Gd_2Ti_2O_7$. The pyrochlore $Gd_2Ti_2O_7$ phase is stable when calcination temperature is as high as 1,000°C, and cell expansion can be observed with rising calcination temperature. The shrinking band gap energy can be attributed to grain growth at high temperature, which can be explained

by quantum size effect. The decreases in BET surface area and pore volume of the composite with increasing calcination temperature are mostly due to the effect of calcination temperature on the supported gadolinium titanate, because the HZSM-5 zeolite is stable at the mentioned thermal treating temperature.

Crystallization of pyrochlore $Gd_2Ti_2O_7$ and the porosity in the loaded $Gd_2Ti_2O_7$ layer are two major factors when we try to investigate the effects of calcination temperature. Well crystallized $Gd_2Ti_2O_7$ has good activity, while shrinking surface area and porosity at high temperature are detrimental to its activity. The $Gd_2Ti_2O_7$/HZSM-5 sample calcined at 800°C has the maximum activity on ofloxacin degradation, due to the above-mentioned complex factors.

4. Conclusions

$Gd_2Ti_2O_7$ was loaded on the surface of HZSM-5 particles through a sol-gel route. The pyrochlore $Gd_2Ti_2O_7$ phase is stable during thermal treatment at temperature as high as 1,000°C. FT-Far IR spectra of $Gd_2Ti_2O_7$/HZSM-5 prove the formation of gadolinium titanate. The shrinking band gap energy of $Gd_2Ti_2O_7$/HZSM-5 can be attributed to grain growth at high temperature. BET surface area reduces from 116.6 to 45.5 m^2/g when calcination temperature increases from 600°C to 1,000°C. Total pore volume is also reduced at high calcination temperature. Both adsorption capacity and photocatalytic activity of $Gd_2Ti_2O_7$/HZSM-5 depend on porous properties of the supported $Gd_2Ti_2O_7$ layer.

Acknowledgment

This work was supported by the Natural Science Foundation of Liaoning Province (No. 2015020186).

References

[1] Z. Zhu, P. Huo, Z. Lu, Y. Yan, Z. Liu, W. Shi, C. Li, H. Dong, Fabrication of magnetically recoverable photocatalysts using g-C_3N_4 for effective separation of charge carriers through like-Z-scheme mechanism with Fe_3O_4 mediator, Chem. Eng. J., 331 (2018) 615–625.

[2] G. Sharma, S. Bhogal, M. Naushad, A. Kumar, F.J. Stadler, Microwave assisted fabrication of La/Cu/Zr/carbon dots trimetallic nanocomposites with their adsorptional vs photocatalytic efficiency for remediation of persistent organic pollutants, J. Photochem. Photobiol., A, 347 (2017) 235–243.

[3] G. Panthi, A. Yousef, N.A.M. Barakat, K.A. Khalil, S. Akhter, Y.R. Choi, H.Y. Kim, Mn_2O_3/TiO_2 nanofibers with broad-spectrum antibiotics effect and photocatalytic activity for preliminary stage of water desalination, Ceram. Int., 39 (2013) 2239–2246.

[4] Z. Li, M. Qi, C. Tu, W. Wang, J. Chen, A.J. Wang, Highly efficient removal of chlorotetracycline from aqueous solution using graphene oxide/TiO_2 composite: properties and mechanism, Appl. Surf. Sci., 425 (2017) 765–775.

[5] D. Pang, L. Qiu, Y. Wang, R. Zhu, F. Ouyang, Photocatalytic decomposition of acrylonitrile with N–F codoped TiO_2/SiO_2 under simulant solar light irradiation, J. Environ. Sci., 33 (2015) 169–178.

[6] G. Plantard, T. Janin, V. Goetz, S. Brosillon, Solar photocatalysis treatment of phytosanitary refuses: Efficiency of industrial photocatalysts, Appl. Catal., B, 115–116 (2012) 38–44.

[7] W.J. Zhang, Y.X. Liu, X.B. Pei, X.J. Chen, Effects of indium doping on properties of xIn-0.1%Gd-TiO_2 photocatalyst synthesized by sol-gel method, J. Phys. Chem. Solids, 104 (2017) 45–51.

[8] W.J. Zhang, Z. Ma, L. Du, L.L. Yang, X.J. Chen, H.B. He, Effects of calcination temperature on characterization and photocatalytic activity of $La_2Ti_2O_7$ supported on HZSM-5 zeolite, J. Alloys Compd., 695 (2017) 3541–3546.

[9] F. Li, K. Yu, L. Lou, Z. Su, S. Liu, Theoretical and experimental study of La/Ni co-doped $SrTiO_3$ photocatalyst, Mater. Sci. Eng. B, 172 (2010) 136–141.

[10] W.J. Zhang, Y.J. Tao, C.G. Li, Effects of PEG4000 template on sol-gel synthesis of porous cerium titanate photocatalyst, Solid State Sci., 78 (2018) 16–21.

[11] Z. Chen, H. Jiang, W. Jin, C. Shi, Enhanced photocatalytic performance over $Bi_4Ti_3O_{12}$ nanosheets with controllable size and exposed {001} facets for Rhodamine B degradation, Appl. Catal., B, 180 (2016) 698–706.

[12] L.M. Lozano-Sánchez, S. Obregón, L.A. Díaz-Torres, S. Lee, V. Rodríguez-González, Visible and near-infrared light-driven photocatalytic activity of erbium-doped $CaTiO_3$ system, J. Mol. Catal., A, 410 (2015) 19–25.

[13] S. Khodadoost, A. Hadi, J. Karimi-Sabet, M. Mehdipourghazi, A. Golzary, Optimization of hydrothermal synthesis of Bismuth titanate nanoparticles and application for photocatalytic degradation of tetracycline, J. Environ. Chem. Eng., 5 (2017) 5369–5380.

[14] W.M. Hou, Y. Ku, Synthesis and characterization of $La_2Ti_2O_7$ employed for photocatalytic degradation of reactive red 22 dyestuff in aqueous solution, J. Alloys Compds., 509 (2011) 5913–5918.

[15] K. Onozuka, Y. Kawakami, H. Imai, T. Yokoi, T. Tatsumi, J.N. Kondo, Perovskite-type $La_2Ti_2O_7$ mesoporous photocatalyst, J. Solid State Chem., 192 (2012) 87–92.

[16] L.L. Zhang, H. Zhong, W.G. Zhang, L. Lu, X.J. Yang, X. Wang, Fabrication of $Dy_2Ti_2O_7$ nanocrystalline at 700°C and its photocatalytic activity, J. Alloys Compd., 463 (2008) 466–470.

[17] P. Guo, X.S. Wang, H.C. Guo, TiO_2/Na-HZSM-5 nano-composite photocatalyst: reversible adsorption by acid sites promotes photocatalytic decomposition of methyl orange, Appl. Catal., B, 90 (2009) 677–687.

[18] V.D. Kumari, M. Subrahmanyam, K.V. Subba Rao, A. Ratnamala, M. Noorjahan, K. Tanaka, An easy and efficient use of TiO_2 supported HZSM-5 and TiO_2 + HZSM-5 zeolite combinate in the photodegradation of aqueous phenol and p-chlorophenol, Appl. Catal., A, 234 (2002) 155–165.

[19] W.J. Zhang, Z. Ma, K.X. Li, L.L. Yang, H. Li, H.B. He, Sol-gel Synthesis of Nano-sized TiO_2 Supported on HZSM-5, Curr. Nanosci., 12 (2016) 514–519.

[20] W. Zhang, L. Du, F. Bi, H. He, A novel $SrTiO_3$/HZSM-5 photocatalyst prepared by sol–gel method, Mater. Lett., 157 (2015) 103–105.

[21] P. Kubelka, F. Munk, Ein Beitrag zur Optik der Farbanstriche, Tech. Phys., 12 (1931) 593–601.

[22] W.J. Zhang, Y.X. Liu, C.G. Li, Photocatalytic degradation of ofloxacin on $Gd_2Ti_2O_7$ supported on quartz spheres, J. Phys. Chem. Solids, 118 (2018) 144–149.

[23] X. Li, B. Li, J. Xu, Q. Wang, X.M. Pang, X.H. Gao, Z.Y. Zhou, J.R. Piao, Synthesis and characterization of Ln-ZSM-5/MCM-41 (Ln = La, Ce) by using kaolin as raw material, Appl. Clay Sci., 50 (2010) 81–86.

[24] L. Zhang, Z. Xing, H. Zhang, Z. Li, X.Y. Wu, X.D. Zhang, Y. Zhang, W. Zhou, High thermostable ordered mesoporous SiO_2–TiO_2, coated circulating-bed biofilm reactor for unpredictable photocatalytic and biocatalytic performance, Appl. Catal., B, 180 (2016) 521–529.

[25] A. Garbout, I.B. Taazayet-Belgacem, M. Férid, Structural, FT-IR, XRD and Raman scattering of new rare-earth-titanate pyrochlore-type oxides $LnEuTi_2O_7$, (Ln=Gd, Dy), Cheminform, 573 (2013) 43–52.

[26] A. Garbout, N. Kallelkchaou, M. Férid, Relationship between the structural characteristics and photoluminescent properties of $LnEuTi_2O_7$ (Ln=Gd and Y) pyrochlores, J. Lumin., 169 (2016) 359–366.

[27] M.A. Butler, Photoelectrolysis and physical properties of the semiconducting electrode WO_2, J. Appl. Phys., 48 (1977) 1914–1920.